Acta Cryst. (1993). A**49**, 80-91

The Resolution Function of Single-Crystal Diffractometers at a Synchrotron-Radiation Source: the Influence of Absorption and Extinction on the FWHM

BY ELISABETH ROSSMANITH

Mineralogisch-Petrographisches Institut der Universität Hamburg, D-2000 Hamburg 13, Grindelallee 48, Germany

(*Received* 10 *April* 1992; *accepted* 9 *June* 1992)

Abstract

For the input of the correct intensity-data-collection parameters - the scan width and the number of steps - the expected full widths at half-maximum of the Bragg intensity profiles (FWHM) for the whole θ range under consideration must be known. These FWHMs depend on the divergence of the incident synchrotron beam, on the monochromator and on the mosaic structure of the sample used. They are also affected by absorption and extinction. A simple but very effective resolution function for a triple-crystal diffractometer, applicable also to single- and double-crystal diffractometers, is given, taking all the dependences mentioned above into account. The calculated FWHMs are compared with the measured ones of three different single-crystal samples, namely the FWHMs of a YIG sphere and an Si sphere, obtained at various wavelengths in the range 0.3 to 2.2 Å with the new Huber four-circle diffractometer set up at HASYLAB and the FWHMs of a CaF_2 sphere, given in the literature and measured with the old five-circle Stoe diffractometer at HASYLAB (DESY, Hamburg, Germany). It is shown that, with use of the proposed resolution function, the beam characteristics - divergence and wavelength spread - as well as the characteristics of the samples - mosaic spread and mosaic block size - can be determined from comparison with experimental FWHMs, measured at different wavelengths.

Introduction

Usually, single-crystal diffractometer set-ups consist in a conventional X-ray tube as the beam source, a single-crystal monochromator and the small single-crystal sample bathed in the beam. Because of the dominant contributions of the divergence and wavelength spread to the peak widths in such equipment, the scan range $\Delta\theta$ for Bragg intensity measurements for these diffractometers is usually calculated in very good agreement with the experiment using the resolution function

$$\Delta\theta = A + B \tan\theta_h, \qquad (1)$$

where the constant term A in (1) is assumed to depend on the crystal shape and mosaicity and on the divergence of the primary beam (A and $\Delta\theta$ are in radians). The second term $B = (\lambda_1 - \lambda_2)/\lambda_2$ takes into account the widening of the reflection due to the split in the Bragg angle θ_h caused by the $K\alpha_{1,2}$ components $\lambda_{1,2}$ of the wavelength λ of the incident beam (Furnas, 1957; Enraf-Nonius, 1982).

However, at a synchrotron-radiation source, the incident X-ray beam has a very small divergence and the monochromator usually consists in two perfect single crystals. Because of the continuous spectrum of the incident beam, the X-ray after monochromatization is truly monochromatic with a wavelength spread of $\Delta\lambda/\lambda$, which depends on the divergence of the beam and on the mosaicity of the monochromator crystals. $\Delta\lambda/\lambda$ is small compared with the term B in (1). At a synchrotron-radiation source, therefore, neither the divergence δ nor the wavelength spread $\Delta\lambda/\lambda$ of the beam impinging on the sample dominate the full width at half-maximum (FWHM) of the Bragg intensity profiles, but the mosaicity of the sample crystal affects the FWHM to the same order of magnitude as the beam characteristics. Thus (1) cannot be used.

The general theory of the double-crystal diffractometer is discussed in detail by, for example, Compton & Allison (1935), Zachariasen (1945) and Laue (1960). The resolution function of a triple-crystal diffractometer is given by, for example, Bubakova, Drahokoupil & Fingerland (1961). Both the double- and triple-crystal spectrometers are described fully by Pinsker (1978). Laktionov *et al.* (1989) complemented the instrumental function of a four-circle X-ray diffractometer with the introduction of the crystal mosaicity. The formulas given by all these authors for the Bragg intensity profiles are not easy to handle for two reasons: firstly, many intensity distribution functions, which are not known exactly in a routine intensity-data-collection experiment, are required for calculation; secondly, the evaluation of these expressions necessitate time-consuming computations of integrals, even if approximations to the intensity distributions are used.

Höche *et al.* (1986) therefore used

$$\Delta\theta = (A^2 + B^2 \tan\theta_h)^{1/2} \qquad (2)$$

0108-7673/93/010080-12$06.00

for least-squares fitting of calculated to measured FWHMs of Bragg reflections obtained at the synchrotron source at HASYLAB. The parameter A in (2) was interpreted as a function of the beam divergence and the mosaic spread of the sample and the parameter B was assumed to be mainly due to the wavelength spread $\Delta\lambda/\lambda$.

Rossmanith (1992*a*) (*R*-92 hereafter) proposed a new concept for the calculation of the FWHMs for single and multiple diffraction within an ideally mosaic crystal sample. It was shown that this concept makes possible an approximate evaluation of FWHMs, in excellent agreement with measured ones, without making any assumptions about the intensity distribution functions involved in the experiment. An extension of this concept for the successive diffraction by two or more crystals, the final one having any degree of perfection or mosaicity, will be given in the following.

The resolution function of the triple-crystal diffractometer

The arrangement of the triple-crystal system used at the synchrotron-radiation source at HASYLAB is given in Fig. 1. The first two crystals I and II serve as monochromators. The sample is positioned at III. The rotation axes of the three crystals lie in the horizontal plane of the diffractometer. All three axes are therefore perpendicular to the plane of the paper in Fig. 1, whereas the normals of the diffracting planes of the three crystals are parallel to the plane of the paper, lying in the vertical plane of the diffractometer.

(*a*) *The characteristics of the beam - divergence and wavelength spread recorded by the sample*

The monochromator consists in two perfect Si crystals in the parallel (1, −1) arrangement (Pinsker, 1978; Laue, 1960), with the scattering vector $\mathbf{h}_{111}$ normal to the rectangular surfaces (80×40 mm) of the 5 mm thick plane-parallel-crystal plates. The wavelength λ is selected from the continuous spectrum of the incident X-ray beam according to the fixed angle θ_{111} (Fig. 1). The monochromatic beam, diffracted by the (111) plane of the first crystal, is diffracted once more by the (111) plane of the second crystal. Owing to the second reflection and the possible shift of the second crystal in the direction **x** (Fig. 1) the path of the beam impinging on the crystal sample and therefore the sample positioning can be held fixed and does not depend on the wavelength.

The geometry of the double-crystal monochromator in reciprocal space is given in Fig. 2. The (111) planes of the two crystals are parallel; the respective reciprocal-lattice vectors are therefore antiparallel. For the determination of the divergence and wavelength spread of the beam reflected successively by the two monochromator crystals, the FWHMs are estimated as a function of the beam characteristics as well as of the mosaicity of the crystal, given in *R*-92.

In *R*-92, § II.*A*.1, it was shown that an ideally perfect crystal sphere with radius r is represented in reciprocal space by the replacement of the lattice 'points' by lattice spheres with radius $\varepsilon = 1/r$. Applying this concept to the two 'very big' ('almost infinite') perfect monochromator crystals, the reciprocal-lattice points of the Si crystals in Fig. 2 can therefore be represented approximately by dimensionless mathematical points. [The applicability of this approximation will be discussed further in (*c*)].

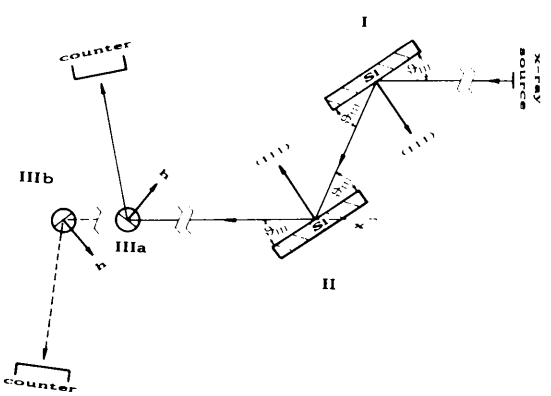

Fig. 1. The arrangement of the triple-crystal system used at the synchrotron-radiation source at HASYLAB.

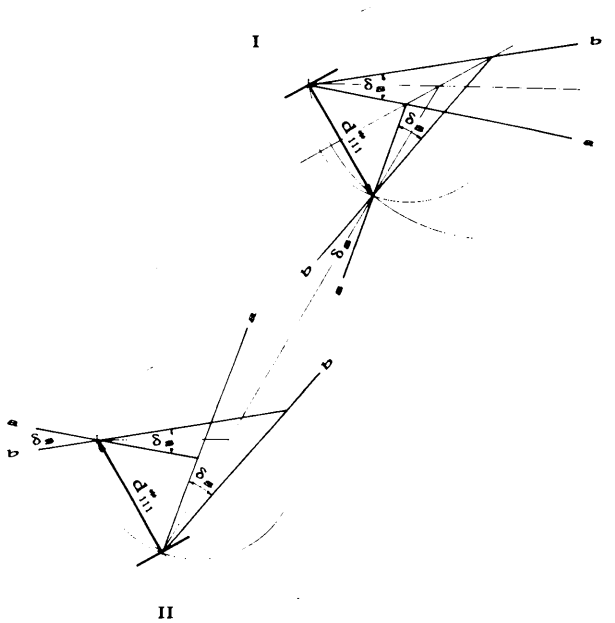

Fig. 2. The geometry of the double-crystal monochromator in reciprocal space.

Table 1. *The Bragg angle and the Darwin width of the* 111 *reflection of the* Si *monochromator crystals and the vertical divergence* δ_s *and wavelength spread* $(\Delta\lambda/\lambda)_s$ *of the synchrotron-radiation beam at HASYLAB* ($E = 4.5$ GeV) *calculated for various wavelengths*

Lattice parameter of Si: $a = 5.4305$ Å.

λ (Å)	θ (°)	$\Delta\theta_D$ (°)	δ_s (°)	$(\Delta\lambda/\lambda)_s$ ($\times 10^{-4}$)
0.3	2.74	0.0004	0.0059	22
0.5608	5.13	0.0007	0.0077	15
0.7107	6.51	0.0009	0.0085	13
1.0	9.18	0.0012	0.0099	11
1.3	11.97	0.0016	0.0110	9
1.5418	14.23	0.0019	0.0118	8
1.8	16.68	0.0022	0.0126	7
2.0	18.60	0.0025	0.0132	7
2.2	20.54	0.0028	0.0138	6

The natural vertical divergence of the beam incident on the monochromator system is mainly determined by the radius R and energy E of the storage ring. For $R = 12.12$ m (DORIS, Hamburg) and $E = 4.5$ GeV (Materlik, 1982), the divergence (°) depends on the wavelength according to

$$\delta_s = 0.008684(\lambda/0.743)^{0.425}. \qquad (3)$$

In Table 1 the divergence defined in (3) is given for various wavelengths λ.

In Fig. 2, each ray between the limiting rays **a** and **b** of the synchrotron-radiation beam with divergence δ_s, incident on the first monochromator crystal I, comprises the whole range of wavelengths of the continuous spectrum. But only those wavelengths of each ray whose corresponding Ewald sphere passes through the zero point of the reciprocal lattice as well as through the point 111 can be diffracted by the (111) plane. The centres of the possible Ewald spheres are the intersection points between the bisector of the reciprocal-lattice vector $\mathbf{h}_{111}$ and the respective incident rays. The maximum wavelength of the reflected beam depends on ray **a**; the minimum wavelength depends on ray **b**. It is obvious from Fig. 2 that the divergence of the reflected beam is equal to the divergence of the incident beam. But the wavelengths of the limiting rays **a** and **b** are different. It is also obvious from Fig. 2 that, in the parallel arrangement of the monochromator crystals, the second reflection affects neither the divergence δ_s nor the wavelengths corresponding to the particular rays within **a** and **b**. With use of the Bragg equation and its derivative, it is easily deduced from Fig. 2 that the wavelength spread is related to the divergence by the expression

$$\begin{aligned}(\Delta\lambda/\lambda)_s &= [\sin(\theta_{111} + \delta_s/2) \\ &\quad - \sin(\theta_{111} - \delta_s/2)]/\sin\theta_{111} \\ &\simeq \delta_s/\tan\theta_{111}, \end{aligned} \qquad (4)$$

where $\Delta\lambda = \lambda_{max} - \lambda_{min}$, λ is the wavelength of the central ray and θ_{111} is the kinematical Bragg angle. Values for the wavelength spread calculated for various wavelengths, using the appropriate δ_s, are also given in Table 1.

However, the divergence δ_{cryst} and wavelength spread $(\Delta\lambda/\lambda)_{cryst}$ recorded by the sample crystal is much smaller than δ_s and $(\Delta\lambda/\lambda)_s$. Since the divergence of the beam emitted by the synchrotron radiation source is not altered by the monochromator system, the actual maximum divergence δ_{max} recorded by the sample can be estimated according to (Fig. 3*a*)

$$\tan(\delta_{max}/2) = (s/2 + r)/L, \qquad (5a)$$

where s is the vertical dimension of the source, r is the radius of the crystal sphere and L is the distance between the source and the sample. It follows from (5*a*) that δ_{max} depends solely on geometrical factors and is independent of the wavelength. The maximum divergence δ_{max} is related to FWHM δ_{cryst} (Fig. 3*b*) by a factor $f \leq 1$:

$$\delta_{cryst} = f\delta_{max}. \qquad (5b)$$

f and therefore δ_{cryst} cannot be calculated exactly because the intensity distribution function $I(\delta)$ of the part of the beam impinging on the crystal is not known. But if f can be estimated experimentally then, from (5) and (4), calculation of δ_{cryst} and $(\Delta\lambda/\lambda)_{cryst}$ for various samples and wavelengths is straightforward. In this case, δ_s has to be replaced by δ_{cryst} in (4).

(*b*) *The FWHM of the crystal sample*

The geometry of the Bragg reflection at the sample positions III*a* and III*b* in reciprocal space is given in Figs. 4(*a*) and (*b*), respectively. In Fig. 4(*a*) the crystal is arranged antiparallel with respect to the second monochromator crystal; in Fig. 4(*b*) it is arranged parallel.

In contrast to the monochromator crystals, whose inclination to the incident beam is given by the fixed angle θ_{111}, the sample crystal is rotated during intensity measurement. Fig. 4 corresponds to Fig. 3(*d*) in *R*-92 except that in the latter it is assumed

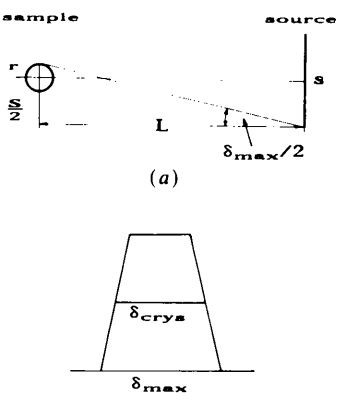

Fig. 3. Derivation of (*a*) δ_{max}, (*b*) δ_{cryst}.

that all the divergent rays impinge on the crystal with the same wavelength spread $\Delta\lambda/\lambda$. In Fig. 4 of this paper the minimum wavelength corresponds to the ray **b** and the maximum wavelength corresponds to the ray **a** of the rays reflected by the monochromator system. This fact mainly affects the FWHMs corresponding to the parallel arrangement given in Fig. 4(*b*).

From the reasoning given in *R*-92, due to the divergence δ_{cryst}, two limiting Ewald spheres have to be drawn, the smallest for ray **a** with radius $r_1^* = 1/\lambda_{max}$ and the largest for ray **b** with radius $r_2^* = 1/\lambda_{min}$.

For simplicity, the crystal is assumed to be composed of perfect spherical mosaic blocks with a mosaic spread η. Owing to the finite radius r of the mosaic blocks, the region in which the corresponding reciprocal-lattice 'sphere' with radius $\varepsilon = 1/r$ is in a reflection position is broadened further. During rotation of the crystal about an axis normal to the plane of the paper, all the reciprocal-lattice 'spheres' are rotated about the zero point O of the lattice. The reciprocal-lattice 'sphere' is first in a reflection position at P_1 and is last in a reflection position at P_2' (see *R*-92 for details). The peak width $\Delta\theta_h$ for the antiparallel arrangement, shown in Fig. 4(*a*), is therefore given by the angle P_1OP_1',

$$\Delta\theta_h = \delta_2 + \delta_{cryst} - \delta_1 + \eta \qquad (6a)$$

with

$$\delta_1 = \arccos\{[r_1^{*2} + d_h^{*2} - (r_1^* - \varepsilon)^2]/(2r_1^* d_h^*)\}, \qquad (6b)$$

$$\delta_2 = \arccos\{[r_2^{*2} + d_h^{*2} - (r_2^* + \varepsilon)^2]/(2r_2^* d_h^*)\}, \qquad (6c)$$

where d_h^* is the length of the reciprocal-lattice vector.

For the parallel arrangement, depicted in Fig. 4(*b*), the expression

$$\Delta\theta_h = |\delta_2 - \delta_{cryst} - \delta_1| + \eta \qquad (7a)$$

is obtained, with $\delta_{1,2}$ defined in (6*b*, *c*) for the case $d_h^* > d_{111}^*$ of Si, and

$$\delta_1 = \arccos\{[r_1^{*2} + d_h^{*2} - (r_1^* + \varepsilon)^2]/(2r_1^* d_h^*)\} \qquad (7b)$$

$$\delta_2 = \arccos\{[r_2^{*2} + d_h^{*2} - (r_2^* - \varepsilon)^2]/(2r_2^* d_h^*)\} \qquad (7c)$$

otherwise. The formula (7*a*) reflects the well known fact that, for d_h^*(sample) = d_h^*(monochromator), the FWHM depends only on the crystal characteristics (mosaic block size and mosaic spread of the crystal; Darwin width of a perfect-crystal plane-parallel plate). Moreover, from Figs. 4(*a*) and (*b*) and from the comparison of (6*a*) with (7*a*), the well known fact can be deduced that the peak width recorded in the parallel arrangement is smaller than that of the antiparallel arrangement.

Insertion of the FWHMs for the divergence δ, the mosaic spread η and the wavelength spread $\Delta\lambda/\lambda$ results in the FWHM $\Delta\theta_h$ of the peak width of the sample. In Figs. 5 and 6, $\Delta\theta_h$ is plotted against θ. The dependence of $\Delta\theta_h$ on the wavelength spread is shown in Fig. 5. The curves of Fig. 5, calculated with $\eta = \delta = \varepsilon = 0$ in (6*a*), correspond to the values of the wavelength spread recorded by a sphere with radius 150 μm [$(\Delta\lambda/\lambda)_{YIG}$ given in Table 2 for various wavelengths]. It is clear from Fig. 5 that the peak

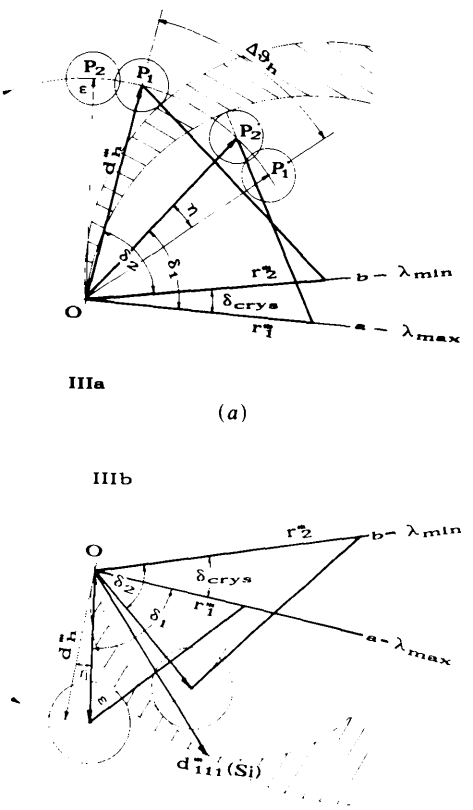

Fig. 4. Geometry of the Bragg reflection at the sample positions (*a*) III*a* and (*b*) III*b* in reciprocal space.

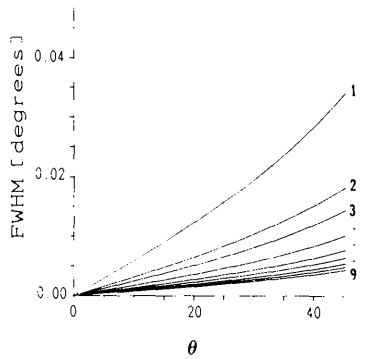

Fig. 5. Dependence of $\Delta\theta_h$ on the wavelength spread for various wavelengths. ($\delta = \eta = \varepsilon = 0$; $\Delta\lambda/\lambda$ calculated according to (4) using δ_{cryst} recorded by a crystal sphere with $r = 150$ μm. See also Table 2(*a*). Curves 1, 2, ..., 9: $\lambda = 0.3$, 0.5608, 0.7107, 1.0, 1.3, 1.5418, 1.8, 2.0, 2.2 Å, respectively.

Table 2. *FWHMs of YIG*

$\delta_{YIG} = 0.0016°$; δ_{YIG} and $(\Delta\lambda/\lambda)_{YIG}$ calculated using (5) and (4) with $f = 0.75$, $L = 37310$ mm, $s = 1.1$ mm, $r_{YIG} = 150$ μm. FWHMs in 10^{-4}°. Interplanar spacings: $d_{004} = 3.095$; $d_{134} = 2.428$ Å. Uncertainty of measured FWHMs ~ half of the step width of the ω scan [$\sim \pm 0.0015°$ in (*b*)].

(*a*) Comparison of the FWHMs of the 004 and 134 reflections of YIG for various wavelengths

λ (Å)	$1/\mu$ (μm)	$(\Delta\lambda/\lambda)_{YIG}$ ($\times 10^{-4}$)	η	h k l	r_{ext} (μm)	$\Delta\theta_D$	$\Delta\theta_{ext}$	$\Delta\theta_c$	$\Delta\theta_o$
0.3	393	5.9	9	0 0 4	-	-	-	-	-
				1 3 4	81.9	<1	3	49	50 (5)
0.5608	70	3.1	13	0 0 4	7.0	7	51	97	100 (5)
				1 3 4	30.7	1	9	59	50 (5)
0.7107	38	2.5	36	0 0 4	5.3	9	68	136	130 (5)
				1 3 4	20.2	1	14	87	80 (5)
1.0	37	1.7	45	0 0 4	3.9	13	92	170	175 (10)
				1 3 4	16.7	2	17	100	90 (10)
1.3	18	1.3	114	0 0 4	2.8	17	128	275	290 (10)
				1 3 4	10.2	2	28	180	180 (10)
1.5418	12	1.1	181	0 0 4	2.3	21	161	376	390 (15)
				1 3 4	7.3	2	40	260	270 (15)
1.8	19	0.9	135	0 0 4	2.2	24	172	341	345 (15)
				1 3 4	9.1	3	33	207	200 (15)
2.0	15	0.8	150	0 0 4	1.9	27	198	381	340 (10)
				1 3 4	7.4	3	41	230	250 (10)
2.2	11	0.8	202	0 0 4	1.7	31	226	462	450 (30)
				1 3 4	-	-	-	-	-

(*b*) Experimental and theoretical FWHMs of YIG for $\lambda = 1.5418$ Å

h k l	θ	F_h	r_{exp} (μm)	$\Delta\theta_{\Delta\lambda,\delta,\eta}$	$\Delta\theta_{ext}$	$\Delta\theta_c$	$\Delta\theta_o$
2 1 1	8.77	101	7.5	208	78	286	270
0 0 4	14.42	773	2.3	214	161	376	390
2 2 4	17.76	566	2.9	219	105	324	345
1 3 4	18.51	110	7.3	220	40	260	270
1 5 2	19.94	187	5.8	221	47	269	270
0 4 4	20.62	187	5.8	222	46	269	285
2 3 5	22.57	148	6.5	225	38	263	270
1 1 6	22.57	222	5.3	225	47	272	270
4 4 4	25.56	813	2.2	229	104	333	315
0 4 6	26.68	805	2.2	231	100	331	330
2 5 5	27.23	145	6.5	231	33	265	260
2 4 6	27.77	643	2.6	232	82	314	300
0 6 6	31.89	106	7.4	239	27	265	285
2 4 8	34.80	558	2.9	243	65	308	300
5 5 6	35.27	127	6.9	244	27	271	270
4 6 6	35.74	507	3.1	245	59	305	285
0 2 10	39.42	171	6.1	252	30	282	300
5 6 7	40.77	124	7.0	255	26	280	285
4 6 8	42.11	497	3.2	257	56	313	285

width due to $\Delta\lambda/\lambda$ increases with the Bragg angle θ according to

$$\Delta\theta \sim (\Delta\lambda/\lambda)\tan\theta. \tag{8}$$

Since δ_{cryst} is constant, the peak width decreases with increasing wavelength according to (4). The variation of $\Delta\theta_h$ with the radius of the mosaic blocks is shown in Fig. 6: the smaller is the radius, the larger is the increase of the curve for small values of θ. The effect of η and δ on $\Delta\theta_h$ does not depend on θ. The entire curve determined by r and $\Delta\lambda/\lambda$ is shifted upwards according to $\delta + \eta$.

(*c*) *The significance of the radius r of the perfect-crystal mosaic blocks*

The mosaic crystal is a model used only in the kinematical theory. The perfect-crystal mosaic blocks are assumed to be small enough for the kinematical approach to be valid, *i.e.* it is assumed that the attenuation of the intensity of the incident X-ray beam due to absorption and extinction within the mosaic blocks is negligibly small. Within the limits of the kinematical

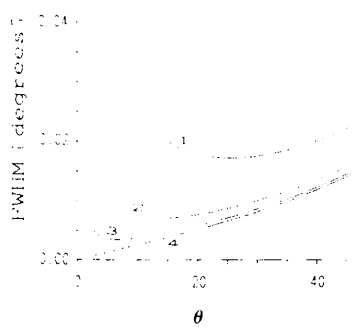

Fig. 6. Dependence of $\Delta\theta_h$ on the radius of the mosaic blocks. Calculated for $\lambda = 0.7107$ Å, $\Delta\lambda/\lambda = 0.000247$, $\delta = \eta = 0$. Curve 1: $r = 1$ μm; curve 2: $r = 5$ μm; curve 3: $r = 20$ μm; curve 4: $r = 5000$ μm.

theory, twice the radius r used in (6) and (7) corresponds to the mean dimension of the mosaic blocks in the sample.

However, in the case of high absorption and extinction and 'large' mosaic blocks, the incident intensity may be totally reflected and/or absorbed during its path through the perfect-crystal block. In this case, the region in reciprocal space for which the reflection condition is fulfilled, *i.e.* the radius of the corresponding reciprocal-lattice 'sphere', is determined by the penetration depth of the incident beam in the mosaic block.

Following Laue (1960), the intensity is attenuated by absorption and extinction according to

$$I = I_0 \exp[-(\mu + \sigma)t], \qquad (9a)$$

where t is the penetration depth in the direction of the beam, μ is the linear absorption coefficient and σ, which is due to extinction, is deduced in the framework of the dynamical theory. In the case of the synchrotron-radiation beam, *i.e.* a beam polarized normal to the reflection plane, σ is related to the extinction length L_{ext} according to

$$\sigma = 1/L_{ext}, \qquad (9b)$$

where L_{ext} is defined by

$$L_{ext} = V_{cell}/(2r_0\lambda|F_h|), \qquad (9c)$$

with $r_0 = 2.818$ fm the classical electron radius, V_{cell} is the volume of the unit cell and F_h is the structure factor [Laue (1960), expressions (23.1), (28.24) and (28.26)]. For $t = 2/(\mu + \sigma)$ the intensity is reduced to about 10% of the incident intensity.

Therefore, in the case when half the penetration depth

$$t/2 = 1/(\mu + \sigma) = r_{ext} \qquad (10a)$$

is smaller than the radius r of the mosaic blocks, the half-penetration depth, r_{ext}, where

$$\varepsilon = 1/r_{ext} = \mu + \sigma, \qquad (10b)$$

has to be used instead of half the mean dimension of the mosaic blocks, r, in (6) and (7).

In *R*-92 [equations (3*a*, *b*, *c*)], it was shown that, for $\Delta\lambda/\lambda = \delta = \eta = 0$, the peak width defined in (6*a*), which is, in this case, solely due to the mosaic-block radius r (or the penetration depth r_{ext}), can be approximated by

$$\Delta\theta_h = 2\varepsilon\lambda/\sin 2\theta. \qquad (11a)$$

In the case of high extinction but negligible absorption, the FWHM can therefore be expressed approximately as

$$\Delta\theta_h = 2\lambda/(L_{ext}\sin 2\theta). \qquad (11b)$$

Values obtained for the peak broadening due to r or r_{ext} of a small (limited) perfect-crystal sphere bathed in the X-ray beam will be compared in the next section with the Darwin width, *i.e.* the width of the diffraction pattern for a plane-parallel-crystal plate in the symmetrical Bragg case, in which the diffracted wave emerges through the entrance surface. The divergence and wavelength spread of the beam, incident on the perfect-crystal plate with unlimited lateral extension and thickness, are assumed to be negligible, $\delta = \Delta\lambda/\lambda \sim 0$. The Darwin width, deduced in the framework of the dynamical theory [Laue (1960) formula (28.29) in connection with (26.49)] is given by

$$\Delta\theta_D = 2\lambda/(2\pi L_{ext}\sin 2\theta) \qquad (12)$$

and is therefore a factor of $1/2\pi$ smaller than (11*b*). The polarization factor p is neglected in (12) since, for synchrotron radiation, $p = 1$.

Values of the Darwin width of the 111 reflection of the Si monochromator for the wavelength used in the experiment are also given in Table 1. For all wavelengths the Darwin width is about one order of magnitude smaller than the divergence of the incident synchrotron beam. The broadening due to the monochromator was therefore neglected in §(*a*).

Comparison of measured and calculated FWHMs

Bragg intensity profiles of various reflections of the cubic YIG (garnet structure) and the cubic Si (diamond structure), measured at various wavelengths, are given by Werner (1992) and by Rossmanith, Werner, Kumpat, Ulrich, Bengel, Eichhorn & Almen (1993). The measurement of the Bragg reflections was carried out in the routine ω-step scanning mode with the Huber four-circle diffractometer at HASYLAB (DESY, Hamburg, Germany). FWHMs of intensity profiles of CaF_2, measured with the Stoe five-circle diffractometer at HASYLAB were reported by Höche *et al.* (1986). Details of the measurement and data reduction are fully described in the above-mentioned papers.

It will be shown in the following that the values of all the experimental FWHMs of all three crystals can be explained by use of the assumption that these crystal spheres consist of one large perfect-crystal block in the core of each sphere, surrounded by many small blocks in the vicinity of the sphere surface, which may be due to mechanical damage during grinding. For such crystals, the condition $r > r_{ext}$ is very often fulfilled. They are therefore very well suited for testing the formulas proposed in the previous section.

(*a*) *The FWHMs of YIG – a case of severe absorption and extinction*

The YIG single crystal, ground to a sphere with radius 150 μm, was supplied by Professor W. Tolksdorf (Philips-Forschungslaboratorium, Hamburg, Germany). The synthetic $Y_3Fe_5O_{12}$ yttrium iron

garnet crystallizes in space group $Ia3d$ with eight formula units per cell [Wyckoff notation: Y^{3+} in 24(c), Fe^{3+} in a 16(a) octahedral site, Fe^{3+} in a 24(d) tetrahedral site, O^{2-} in 96(h)]. The cell dimension is 12.381 Å.

The measured intensity profiles of YIG were re-analysed with the help of the program *PROFIL* (Rossmanith, 1992*b*). The FWHMs were obtained, fitting an asymmetric modified pseudo-Voigt distribution to the measured intensity profiles of the Bragg reflections.

Because of the special positions of the metal atoms in the structure, there are rather weak reflections with contributions from O atoms alone (*e.g.* $F_{134} = 110$) and very strong reflections with contributions from all atoms (*e.g.* $F_{004} = 773$). (The isotropic temperature parameters used for the calculation of the structure factors F_h are $B_{O,Fe,Y} = 0.42$, 0.35, 0.30 Å^2.) In particular, the strong reflections are therefore known to be affected by severe extinction (Bonnet, Delapalme, Fuess & Thomas, 1975). Because of the K-absorption edge of Fe, the absorption for wavelengths greater than 1 Å is appreciable. The FWHMs of the YIG-crystal sphere are therefore very well suited for the examination of the formulas for large perfect-crystal mosaic blocks with $r > r_{ext}$ given in the preceding chapter.

The FWHMs of YIG for wavelengths between 0.3 and 2.2 Å, obtained from profile analysis, are presented in Fig. 7 and Table 2. It is obvious from Fig. 7 that there is a large spread in the FWHMs of YIG; the smallest width (0.003°) was obtained for the 211 reflection with $\lambda = 0.3$ Å, the largest measured width (=0.045°) was obtained for the 004 reflection with $\lambda = 2.2$ Å. In Table 2(b) the complete set of widths measured at $\lambda = 1.5418$ Å is compared with calculations. In Table 2(a) measured and calculated widths of the strong 004 reflection are compared with those of the weak 134 reflection for all the wavelengths used in the experiment.

For $\lambda = 0.3$ Å the absorption coefficient μ is small, *viz* $1/\mu = 393$ μm (see Table 2a) is larger than the diameter of the YIG sphere. Moreover, owing to the small wavelength [see (9c)], the extinction lengths of the reflections and consequently the corresponding r_{ext} defined in (10a) are large. With the assumption that the crystal model introduced above is appropriate to YIG, it is implied that the incident beam can deeply penetrate the large core mosaic block. In the case of the rather weak 134 reflection, for example, $r_{ext} =$ 81.9 μm (see Table 2), the diffraction therefore mainly takes place in the core mosaic block, whose radius is assumed to be larger than r_{ext}. The broadening of the intensity profiles due to the enlargement of the reciprocal-lattice points to 'spheres' is consequently negligibly small, being $\Delta\theta_{exp} = 0.0003°$ for the 134 reflection and lying between 7 and less than 1×10^{-4}° for all the other reflections. As a consequence of the

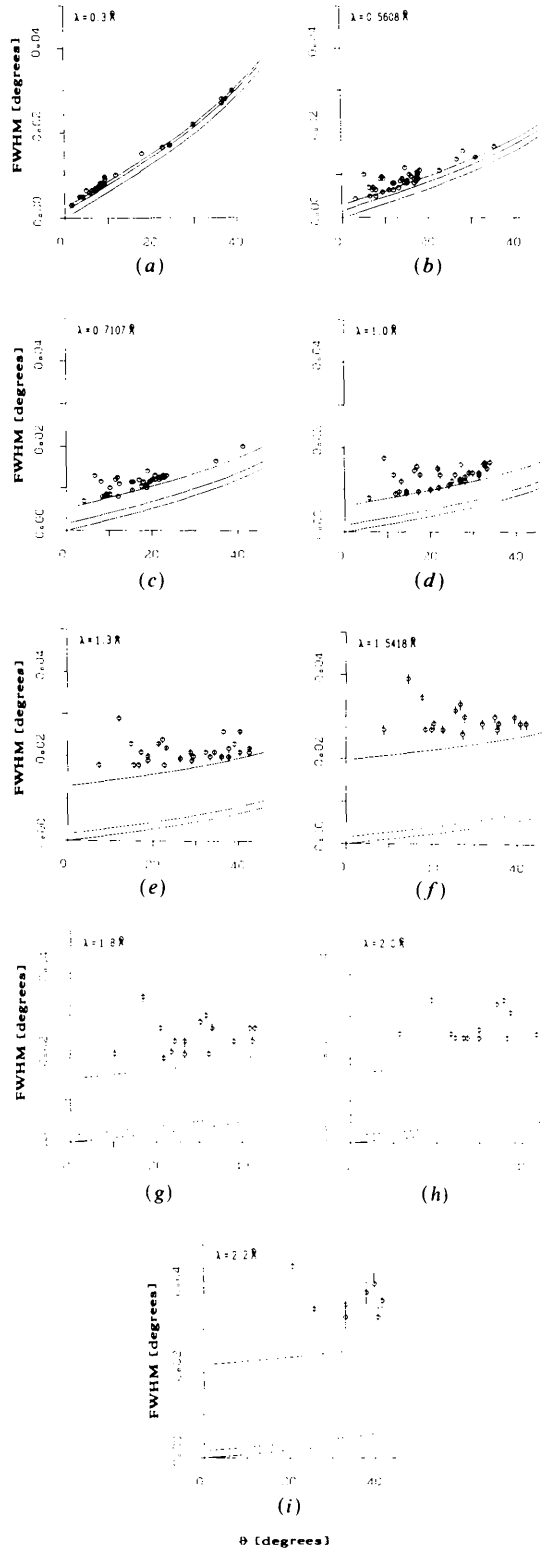

Fig. 7. FWHMs of YIG for various wavelengths. Symbols correspond to experimental FWHMs. Lowest curve: calculated width due to $(\Delta\lambda/\lambda)_{YIG}$ only; middle curve: calculated width due to $(\Delta\lambda/\lambda)_{YIG}$ and δ_{YIG}; upper curve: calculated width due to $(\Delta\lambda/\lambda)_{YIG}$, δ_{YIG} and η.

proposed crystal model the FWHMs of Fig. 7(*a*) should therefore be mainly due to $\Delta\lambda/\lambda$, δ and η, *i.e.* the measured FWHMs should be parallel to a function that is similar to the curves given in Fig. 5.

The measurement at $\lambda = 0.3$ Å was therefore used to adjust the factor f, defined in (5*b*). For this purpose, δ and therefore $\Delta\lambda/\lambda$, recorded by the YIG sphere, were calculated according to (5) and (4), with $s =$ 1.1 mm, $L = 37310$ mm and $r_{YIG} = 150$ μm and the middle curve of Fig. 7(*a*) was calculated according to (6) with $\varepsilon = \eta = 0$. The best agreement between the slope of the curve and the measured FWHMs was obtained with $f = 0.75$, resulting in $\delta_{YIG} = 0.0016°$ and $\Delta\lambda/\lambda = 0.00059$. Since δ_{YIG} does not depend on the wavelength, once f has been adjusted, the wavelength spread for all the other wavelengths used in the experiment can be calculated according to (4), with use of the Bragg angles of the monochromator system (see Table 1). The results for $(\Delta\lambda/\lambda)_{YIG}$, obtained in this way, are given in Table 2(*a*). They have been used also to produce Fig. 5.

In Figs. 7(*a*)-(*i*), the lowest curve in each diagram, which passes through the origin, represents the calculated $\Delta\theta_h$ due to the wavelength spread $\Delta\lambda/\lambda$ only and corresponds to the appropriate curve in Fig. 5. The middle curve is due to $\Delta\lambda/\lambda$ plus the divergence δ and the uppermost curve corresponds to the FWHM due to $\Delta\lambda/\lambda$, δ and the mosaic spread η.

With the assumption of the perfect-crystal model introduced above and with knowledge of a value for the factor f, the parameters δ_{YIG}, $(\Delta\lambda/\lambda)_{YIG}$ and $\varepsilon = 1/r_{ext}$ can therefore be calculated for all reflections at all wavelengths from only the geometry of the experimental equipment and the structure of the sample. The parameter η, which is still unknown, can consequently be determined for each wavelength by use of the relation

$$\eta = \sum_n (\Delta\theta_o - \Delta\theta_{\Delta\lambda,\delta,\varepsilon})/n, \qquad (13)$$

where $\Delta\theta_o$ is the measured FWHM and $\Delta\theta_{\Delta\lambda,\delta,\varepsilon}$ is the FWHM calculated according to (6), with the parameters $(\Delta\lambda/\lambda)_{YIG}$, δ_{YIG} and r_{ext}, but with $\eta = 0$. It is clear from (13) that the mosaic spread η obtained in this way is affected by the error of the measured values.

The mosaic spread obtained according to (13) is also given in Table 2(*a*) for all the wavelengths used in the experiment and corresponds to the distance between the middle and uppermost curves in Figs. 7(*a*)-(*i*). Whereas the very small values obtained for η at $\lambda = 0.3$ and 0.5 Å may be due only to the uncertainties of the measurement, values of η for the other wavelengths seem to have physical significance. η increases with decreasing $1/\mu$, having a local maximum for $\lambda = 1.5418$ Å in the vicinity of the K-absorption edge of Fe. r_{ext} (see Table 2), which is a measure of the penetration depth in the crystal, is large for small wavelengths but is only a few μm for larger wavelengths. In the case of small wavelengths, therefore, diffraction occurs mainly in the large core mosaic block, corresponding to $\eta \sim 0$, whereas at larger wavelengths diffraction occurs in the small mosaic blocks at the surface of the sphere, which are tilted relative to each other according to the mosaic spread η.

The mosaic spread η can only successfully be determined from (13), provided that the difference between the measured FWHMs, $\Delta\theta_o$, and the calculated FWHMs, $\Delta\theta_{\Delta\lambda,\delta,\eta}$, corresponding to the uppermost curve in Figs. 7(*a*)-(*i*), can be entirely related to the peak broadening $\Delta\theta_{exp}$ due to the penetration depth r_{ext} of the X-ray beam in the crystal, *i.e.* provided that the width calculated according to (10) and (6) is an adequate approximation.

In Table 2(*b*) the measured FWHMs, $\Delta\theta_o$, of Fig. 7(*f*) are compared with the theoretical ones, calculated for $\lambda = 1.5418$ Å. $\Delta\theta_c$ is the FWHM calculated with the parameters $\Delta\lambda/\lambda$, δ and η given in Table 2(*a*) and r_{ext} given in the fourth column of Table 2(*b*). Therefore, $\Delta\theta_{exp} = \Delta\theta_c - \Delta\theta_{\Delta\lambda,\delta,\eta}$ can be calculated, which is the contribution to the width due to absorption and extinction. $\Delta\theta_{exp}$ can also be estimated to a very good approximation using $\varepsilon = 1/r_{ext}$ in (11*a*).

It can be seen from Table 2 that, at the chosen wavelength and for all reflections, the contribution $\Delta\theta_{ext}$ is considerable. According to (11*a*) and Fig. 6, $\Delta\theta_{ext}$ is large for small r_{ext} and small Bragg angles. The largest contribution is found for the very strong 004 reflection, being of the same order of magnitude as the broadening due to $\Delta\lambda$, δ and η. But, owing to the small Bragg angle, the contribution for the weak 211 reflection is also considerably large. Comparison of $\Delta\theta_c$ and $\Delta\theta_o$ shows an excellent agreement between the measured and calculated FWHMs of all reflections, $\Delta\theta_o - \Delta\theta_c$ being comparable to the uncertainty of the measurement, indicating that $\Delta\theta_o - \Delta\theta_{\Delta\lambda,\delta,\eta}$ is a function of the penetration depth r_{ext} and that the expressions (10*a*), (10*b*) in connection with (6*a*)-(6*c*) are very well suited for an approximate calculation of FWHMs of a spherical sample consisting of mosaic blocks with $r > r_{ext}$.

Similar satisfactory results are obtained for all the other FWHMs represented in Figs. 7(*a*)-(*i*). This is demonstrated in Table 2(*a*), where the very strong 004 reflection is compared with the weak 134 reflection. For all wavelengths the agreement between $\Delta\theta_o$ and $\Delta\theta_c$ for both reflections is surprisingly good, despite the simple theory underlying the calculations. The greatest deviation between measurement and calculation is found for large wavelengths, where r_{ext} varies between ~2 μm for the strong reflections and ~7 μm for the weak reflections. This deviation can be explained by the reasonable assumption that the mosaic spread in the vicinity of the sphere surface

depends to a high degree on the penetration depth of the X-ray beam as well as on the part of the crystal surface illuminated by the incident beam. Under such circumstances the mosaic spread can no longer be supposed to be a constant for all reflections.

In the literature, the 'dynamical perfect-crystal peak broadening' is frequently assumed to be of the order of the Darwin width $\Delta\theta_D$, defined in (12), and is therefore usually neglected in approximations for the FWHMs as given, for example, in (2). But Table 2(*a*) indicates unambiguously that the Darwin width, which is given in the seventh column, is an inadequate approximation for a crystal sphere bathed in an incident beam, *i.e.* for the routine experimental arrangement in crystal structure analysis. Moreover, Table 2(*a*) makes clear that $\Delta\theta_{ext}$, which contributes about 50% to the width of the strong 004 reflection, cannot be neglected in calculating FWHMs.

The very good agreement between the measured and calculated FWHMs of the YIG crystal confirms the proposed crystal model and the formulas given for $\Delta\theta_h$ in the preceding section. It is obvious from the figures and tables that, whereas for small wavelengths the width is mainly determined by the beam characteristics, for large wavelengths the broadening is mainly due to the characteristics of the sample, $\Delta\theta_{ext} + \eta$.

(*b*) *The FWHMs of* Si - *a case of severe extinction but low absorption*

The Si single crystal, ground to a sphere with radius 180 μm, was also supplied by Professor W. Tolksdorf (Philips-Forschungslaboratorium, Hamburg, Germany). Si crystallizes in space group $Fd3m$ with the eight atoms in the unit cell in special positions [Wyckoff notation: 8(*a*)]. The cell dimension is 5.431 Å.

As in the case of YIG, the FWHMs $\Delta\theta_o$ of Si were estimated using the program *PROFIL*. The experimental $\Delta\theta_o$ for the different wavelengths are given in Fig. 8. Selected FWHMs are also listed in Table 3(*a*). Since the factor f is already known from the analysis of the YIG data, the divergence δ_{Si} and wavelength spread $(\Delta\lambda/\lambda)_{Si}$, recorded by the Si sphere, can be calculated according to (5) and (4). The results are given in Table 3(*a*). Therefore, the lowest and middle curves in Figs. 8(*a*)-(*f*), which correspond to the respective curves in Figs. 7(*a*)-(*f*), can be drawn. r_{ext}, which is also given in Table 3(*a*) for the reflections that are most affected by extinction, can be calculated with the help of Tables 3(*a*) and (*b*), in which the linear absorption coefficient, the interplanar spacings and structure factors of these reflections are listed. (Isotropic temperature parameter $B_{Si} = 0.45$ Å^2.)

It is obvious from Fig. 8(*a*) that, as in the case of YIG, for the wavelength $\lambda = 0.3$ Å all the measured FWHMs are in very good agreement with the middle and upper curves, which almost coincide at this wavelength. From Fig. 8(*a*) it may therefore be deduced that the FWHMs are mainly due to $\Delta\lambda/\lambda + \delta$ and that the corresponding mosaic spread η as well as the broadening due to extinction and absorption, $\Delta\theta_{ext}$, of all the reflections are negligible. The smallest value for the penetration depth, $2r_{ext} = 45$ μm, was found for the 044 reflection; the largest, $2r_{ext} = 893$ μm, was found for the 12,12,12 reflection. If it is assumed that the Si crystal also consists of one large core mosaic block, surrounded by small blocks at the crystal surface, and that the diameter of the core mosaic is of the order of the diameter of the crystal sphere, $\Phi = 360$ μm, it follows that the largest value of $\Delta\theta_{ext}$, obtained for $\lambda = 0.3$ Å (see Table 3*a*) is $\Delta\theta_{ext} = 0.0005°$, and the smallest value is less than 0.0001°, in agreement with the experiment. The

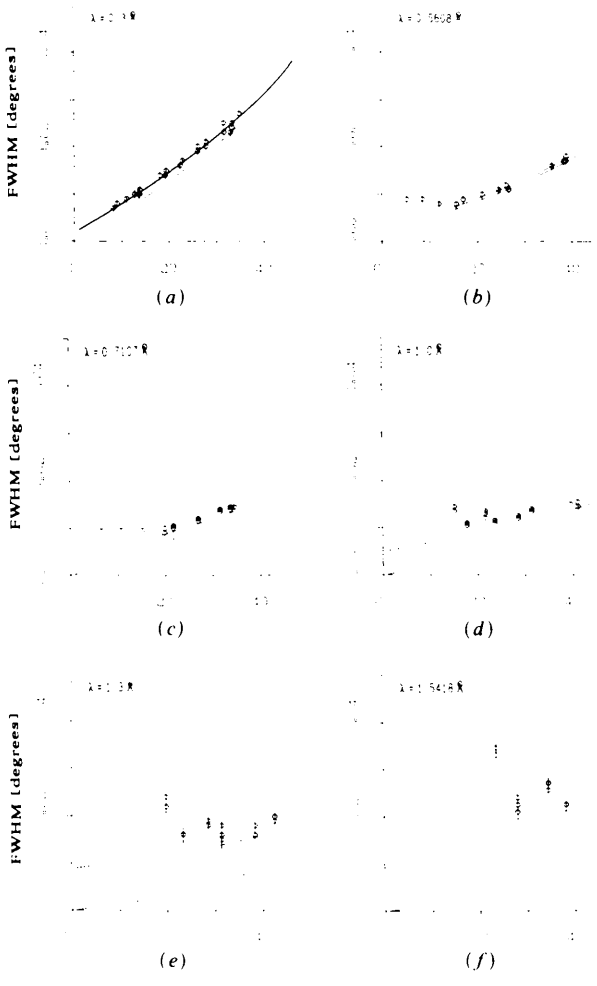

Fig. 8. FWHMs of Si for various wavelengths. Symbols correspond to experimental FWHMs. Lowest curve: calculated width due to $(\Delta\lambda/\lambda)_{Si}$ only; middle curve: calculated width due to $(\Delta\lambda/\lambda)_{Si}$ and δ_{Si}; upper curve: calculated width due to $(\Delta\lambda/\lambda)_{Si}$, δ_{Si} and η.

Table 3. *Results for* Si

$\delta_{Si} = 0.0017°$; δ_{Si} and $(\Delta\lambda/\lambda)_{Si}$ calculated with $f = 0.75$, $L = 37\,310$ mm, $s = 1.1$ mm, $r_{Si} = 180$ μm. FWHMs in 10^{-4} °.

(*a*) Comparison of FWHMs of Si reflections for various wavelengths

λ (Å)	$1/\mu$ (μm)	$(\Delta\lambda/\lambda)_{YIG}$ ($\times 10^{-4}$)	η	*h k l*	r_{ext} (μm)	$\Delta\theta_{ext}$	$\Delta\theta_c$	$\Delta\theta_o$
0.3	6671	6.1	2	0 4 4	22.4	5	79	80 (10)
0.5608	1309	3.3	6	1 1 1	8.5	42	82	90 (10)
				0 2 2	7.5	30	80	90 (10)
				0 0 4	8.9	18	80	80 (10)
0.7107	667	2.6	17	1 1 1	6.7	54	104	95 (5)
				0 2 2	5.9	38	100	95 (5)
				0 0 4	7.0	23	97	95 (5)
1.0	248	1.8	34	0 2 2	4.1	55	134	142 (5)
				1 1 3	6.3	32	116	108 (5)
				0 0 4	4.9	34	126	128 (5)
				3 3 1	7.3	21	118	113 (5)
1.3	116	1.4	73	0 2 2	3.1	74	193	227 (20)
				1 1 3	4.7	43	168	160 (20)
				0 0 4	3.7	47	181	183 (20)
				3 3 1	5.5	30	170	162 (20)
				1 1 5	6.3	24	178	165 (20)
				0 4 4	4.9	31	195	198 (20)
1.5418	70	1.2	141	0 2 2	2.6	92	279	335 (15)
				1 1 3	3.9	54	248	225 (15)
				0 0 4	3.1	61	266	260 (15)
				3 3 1	4.6	40	252	225 (15)

(*b*) Interplanar spacings and structure factors of the Si reflections

h k l	d_h (Å)	F_h
1 1 1	3.137	59.07
0 2 2	1.921	67.74
1 1 3	1.638	44.34
0 0 4	1.358	56.57
3 3 1	1.246	37.83
1 1 5	1.045	32.90
0 4 4	0.960	42.80

vanishingly small η value can again be explained by the fact that diffraction takes place mainly in the large core mosaic block.

The excellent agreement between the middle curve and the experimental FWHMs in Fig. 8(*a*) confirms the fact that the factor *f*, which was fitted to the YIG data, is also applicable to the Si data. Moreover, in accordance with the prediction, the slopes of the experimental FWHMs, shown in Figs. 8(*a*)-(*f*), decrease with increasing wavelengths. It is due to the decreasing slope that, for example, the width for $\theta \sim 40°$ in Fig. 8(*d*), $\Delta\theta_h = 0.015°$, is half that in Fig. 8(*a*), $\Delta\theta_h = 0.03°$, confirming the fact that the divergence recorded by the crystal, δ_{cryst}, depends according to (5) solely on geometrical factors and is independent of the wavelength.

The mosaic spread η can be fitted to the data in the same way as for the YIG crystal with use of (13). It should be pointed out that η is the only parameter that was fitted in the case of Si; all the other parameters - δ_{Si}, $(\Delta\lambda/\lambda)_{Si}$ and r_{ext} - are calculated from the geometry of the experiment and the structure of the Si example. As in the case of YIG, the very small values of η for small wavelengths [Figs. 8(*a*) and (*b*)] are probably due to the uncertainties of the measurement, whereas for large wavelengths, where r_{ext} is again small (see Table 3*a*) and diffraction takes place in the vicinity of the surface, η is the mosaic spread of the small mosaic blocks, due to damage from grinding the Si sphere.

For wavelengths ≥ 0.5 Å, r_{ext} (see Table 3*a*) is small and consequently $\Delta\theta_{exp}$ is considerable for all reflections in the low-θ region. As can be seen from Figs. 8(*b*)-(*f*), the broadening due to extinction cannot be neglected for larger wavelengths. This is especially obvious from Figs. 8(*b*) and (*c*), in which an enlargement of the width with decreasing Bragg angle, similar to that presented in Fig. 6, is observed. This enlargement cannot be explained by an alternative choice of the parameters δ, $\Delta\lambda/\lambda$ and η, but it is well accounted for by $\Delta\theta_{ext}$.

For the reflections most affected by $\Delta\theta_{ext}$, the calculated and observed FWHMs are compared in Table 3(*a*). Although the mosaic spread may vary for different reflections in the case of small r_{ext}, the agreement between theory and experiment, especially for small wavelength, *i.e.* small η, is satisfactory.

(*c*) *The FWHMs of* CaF_2 *- comparison with results given in the literature*

Höche *et al.* (1986) analysed the FWHMs of CaF_2 with the aim of determining the mosaic spread of the sample. Two crystal spheres with radii 45 and 3 μm

were investigated with synchrotron radiation at HASYLAB. The X-ray beam was monochromatized by a flat Ge (111) double monochromator. The measurements were carried out with the wavelengths $\lambda = 0.917$ and 1.714 Å.

CaF_2 crystallizes in space group $Fm3m$ with Ca in the special position 4(a) and F in the special position 8(c) (Wyckoff notation). The cell dimension is 5.45 Å. Because of the special positions of the atoms, reflections with $h+k+l=4n+2$ are very weak; reflections with $h+k+l=4n$ are strong. (Isotropic temperature parameter $B_{Ca,F} = 1.08$ Å^2.)

The results obtained with the 3 μm crystal are not considered here since it cannot be deduced from the paper by Höche *et al.* (1986) how the FWHMs of the reflection profiles, 'which were often divided in separate peaks', have been determined. The results given for the 45 μm crystal are reproduced in Fig. 9 and Table 4.

The curves in Fig. 9 have the same meaning as those in Figs. 7 and 8. Since the monochromator system is different from that used for the YIG and Si measurements, the factor f, obtained for the Si monochromator cannot be used. Therefore, in the case of CaF_2, two parameters have to be adjusted: the factor f, determining the divergence δ and the slope of the curves in Fig. 9, and the mosaic spread η. The best agreement between experimental and theoretical FWHMs was obtained with $f = 1$. The corresponding δ_{CaF_2} and $(\Delta\lambda/\lambda)_{CaF_2}$ are given in the heading of Table 4(a).

With the assumption of a crystal model for the CaF_2 sphere similar to that of YIG and Si, *i.e.* the crystal sphere is assumed to consist of one large perfect core block surrounded by small blocks near the surface of the sphere, the radius of the reciprocal-lattice 'spheres' is given by $\varepsilon = 1/r_{ext}$ and the mosaic spread can be calculated according to (13). The mosaic spread obtained in this way for $\lambda = 0.917$ Å, $\eta = 0.0173°$, is about four to five times larger than the mosaic spread of YIG and Si at the same wavelength. Apart from the structure dependence, this large η may be due to the smaller radius, *i.e.* the relatively larger surface region of the CaF_2 sphere.

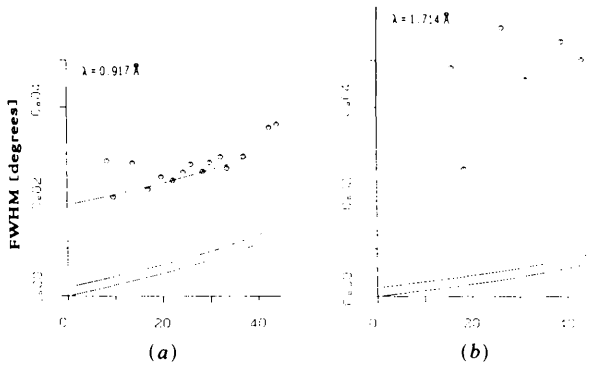

Fig. 9. FWHMs of CaF_2. Symbols correspond to experimental FWHMs given by Höche *et al.* (1986). (a) Lowest curve: calculated width due to $(\Delta\lambda/\lambda)_{CaF_2}$ only; middle curve: calculated width due to $(\Delta\lambda/\lambda)_{CaF_2}$ and δ_{CaF_2}; upper curve: calculated width due to $(\Delta\lambda/\lambda)_{CaF_2}$, δ_{CaF_2} and η. (b) Lower curve: calculated width due to $(\Delta\lambda/\lambda)_{CaF_2}$ only; upper curve: calculated width due to $(\Delta\lambda/\lambda)_{CaF_2}$ and δ_{CaF_2}.

Table 4. *Experimental and theoretical FWHMs of* CaF_2

(a) $\lambda = 0.917$ Å

$\delta_{CaF_2} = 0.0018°$ and $(\Delta\lambda/\lambda)_{CaF_2} = 0.00023°$, calculated with $f = 1.0$, $L = 37310$ mm, $s = 1.1$ mm, $r_{CaF_2} = 45$ μm; $\eta = 0.0173°$, $1/\mu = 147$ μm. FWHMs in 10^{-4}°.

h k l	θ	F_h	r_{ext} (μm)	$\Delta\theta_{ext}$	$\Delta\theta_c$	$\Delta\theta_o$
1 1 1	8.4	60.6	5.0	73	284	286 (14)
2 0 0	9.7	1.3	$92.5 \gg r_{CaF_2}$	7	221	209 (15)
2 2 0	13.8	90.9	3.4	68	291	281 (45)
2 2 2	16.9	6.1	37.9	5	236	225 (17)
4 0 0	19.7	64.7	4.7	35	273	252 (18)
4 2 0	22.1	7.5	32.4	5	249	245 (20)
4 2 2	24.3	50.2	6.0	23	274	261 (23)
5 1 1	25.9	27.2	10.7	13	267	278 (12)
4 4 0	28.4	41.3	7.2	17	279	263 (35)
5 3 1	29.9	23.4	12.3	10	276	282 (21)
6 2 0	32.2	35.2	8.4	14	287	294 (15)
5 3 3	33.5	20.6	13.8	8	286	270 (24)
7 1 1	36.9	18.3	15.3	7	297	294 (20)
8 0 0	42.3	24.1	12.0	9	319	356 (32)
8 2 0	43.9	6.4	36.7	3	320	363 (24)

(b) $\lambda = 1.714$ Å

$\delta_{CaF_2} = 0.0018°$ and $(\Delta\lambda/\lambda)_{CaF_2} = 0.00012°$, calculated with $f = 1.0$, $L = 37310$ mm, $s = 1.1$ mm, $r_{CaF_2} = 45$ μm; $1/\mu = 25.6$ μm. FWHMs in 10^{-4}°.

h k l	θ	r_{ext} (μm)	$\Delta\theta_{ext}$	$\Delta\theta_{\Delta\lambda/\lambda,\delta}$	η	$\Delta\theta_o$
1 1 1	15.8	2.5	150	38	297	485 (21)
2 0 0	18.3	21.5	15	41	212	269 (16)
2 2 0	26.4	1.7	143	53	373	569 (33)
3 1 1	31.4	3.4	64	61	334	459 (31)
4 0 0	39.0	2.4	85	75	381	541 (27)
3 3 1	43.3	4.3	46	84	372	502 (30)

The comparison of the calculated and experimental FWHMs presented in Table 4(a) shows excellent agreement between theory and measurement. In particular, the large broadening due to extinction, $\Delta\theta_{ext}$, for the strong 111 and 220 reflections and the small contributions $\Delta\theta_{ext}$ for the very weak 200, 222 and 420 reflections are predicted correctly, confirming once more the usefulness of the crystal model and the formulas used.

The FWHMs given by Höche *et al.* (1986) for $\lambda = 1.714$ Å, which they could not analyse ['owing to strong extinction no unique function (2) can be derived'] are reproduced in Fig. 9(b) and Table 4(b). The contributions to the width due to the beam characteristics, $\Delta\theta_{\delta,\Delta\lambda/\lambda}$, and due to the penetration depth r_{ext}, $\Delta\theta_{ext}$, are also given in Table 4(b). It is obvious from this table that for small Bragg angles the contribution due to absorption and extinction considerably exceeds the contribution due to the beam characteristics. The mosaic spread, calculated individually for each reflection, $\eta_{hkl} =$

$(\Delta\theta_o - \Delta\theta_{\delta,\Delta\lambda/\lambda} - \Delta\theta_{exp})_{hkl}$, is given in the sixth column of Table 4(*b*). In accordance with the proposed crystal model, the smallest η is found for the very weak 200 reflection, for which the penetration depth of the incident beam is comparatively very large, being about half the diameter of the crystal sphere. The fluctuation of η for the other reflections with r_{ext} between 1.7 and 4.3 μm may once more be due to the experimental error as well as to the variable local values of η for different parts of the sphere surface illuminated by the incident ray.

Concluding remarks

In the preceding section it was shown that, using the proposed resolution function, the beam characteristics - divergence and wavelength spread - as well as the characteristics of the sample - mosaic spread and mosaic block size - can be determined from comparison with experimental FWHMs, measured at different wavelengths. It was also shown that the mosaic spread for samples with high absorption and/or extinction is no longer constant, but may vary appreciably for different reflections. The integrated intensities of the reflections measured with synchrotron radiation are strongly dependent on the varying - and therefore unknown - mosaic structure of the sample. The difficulty of obtaining integrated intensities with sufficient accuracy using synchrotron radiation may partly be due to this fact.

This work was funded by the German Minister of Research and Technology (Förderkennzeichen: 05 405IBB).

References

BONNET, M., DELAPALME, A., FUESS, H. & THOMAS, M. (1975). *Acta Cryst.* B31, 2233-2240.
BUBAKOVA, R., DRAHOKOUPIL, J. & FINGERLAND, A. (1961). *Czech. J. Phys.* B11, 205-222.
COMPTON, A. H. & ALLISON, S. K. (1935). *X-rays in Theory and Experiment.* Princeton, New Jersey: van Nostrand.
Enraf-Nonius (1982). *CAD-4 User's Manual*, ch. XI, p. 7. Enraf-Nonius, Delft, The Netherlands.
FURNAS, T. C. (1957). *Single-Crystal-Orienter Instruction Manual.* Milwaukee: General Electric Company.
HÖCHE, H. R., SCHULZ, H., WEBER, H.-P., BELZNER, A., WOLF, A. & WULF, R. (1986). *Acta Cryst.* A42, 106-110.
LAKTIONOV, A. V., CHULICHKOV, A. I., CHULICHKOVA, N. M., FETISOV, G. V., PYTEV, YU. P. & ASLANOV, L. A. (1989). *J. Appl. Cryst.* **22**, 315-320.
LAUE, M. (1960). *Röntgenstrahlinterferenzen.* Frankfurt am Main: Akademische Verlagsgesellschaft.
MATERLIK, G. (1982). *Uses of Synchrotron Radiation in Biology*, edited by H. B. STUHRMANN, ch. 1, pp. 1-21. New York: Academic Press.
PINSKER, Z. G. (1978). *Dynamical Scattering of X-rays in Crystals.* Berlin, Heidelberg, New York: Springer-Verlag.
ROSSMANITH, E. (1992*a*). *Acta Cryst.* A48, 596-610.
ROSSMANITH, E. (1992*b*). *PROFIL*, a program for intensity profile analysis. Unpublished.
ROSSMANITH, E., WERNER, M., KUMPAT, G., ULRICH, G., BENGEL, K., EICHHORN, K. & ALMEN, H. (1993). In preparation.
WERNER, M. (1992). Diplomarbeit, Univ. Hamburg, Germany.
ZACHARIASEN, W. H. (1945). *Theory of X-ray Diffraction in Crystals*, pp. 99-108. New York: John Wiley.

Acta Cryst. (1993). A49, 91-97

X-ray Scattering Factors of Oxygen and Sulfur Ions: an *Ab Initio* Hartree–Fock Calculation

BY PATRICK AZAVANT AND ALBERT LICHANOT

Laboratoire de Chimie Structurale, URA 474, *Université de Pau et des Pays de l'Adour, IFR, rue Jules Ferry*, 64000 *Pau, France*

(*Received* 20 *March* 1992; *accepted* 12 *June* 1992)

Abstract

The electronic structures of crystalline lithium oxide and lithium sulfide have been theoretically investigated within the Hartree-Fock approximation. X-ray static structure factors are calculated and scattering factors of O^{2-} and S^{2-} ions are deduced following the theoretical model that uses standard scattering curves for the Li^+ ion.

0108-7673/93/010091-07$06.00

Introduction

The O^{2-}, S^{2-}, N^{3-}, ... ions are known to be unstable when free* (Holbrook, Sabry-Grant, Smith & Tandel, 1990) and they present severe convergence problems in the Hartree-Fock (HF) calculation. To obtain the

* The second molar electron affinities of atomic oxygen and sulfur at 0 K are 599 (10) and 416 (10) kJ mol^{-1}, respectively.